Measurement of TeV muon energy loss in iron

W. K. Sakumoto, P. de Barbaro, A. Bodek, H. S. Budd, and B. J. Kim
Department of Physics and Astronomy, University of Rochester, Rochester, New York 14627

F. S. Merritt, M. J. Oreglia, H. Schellman,* and B. A. Schumm†
Enrico Fermi Institute and Department of Physics, University of Chicago, Chicago, Illinois 60637

K. T. Bachmann,‡ R. E. Blair,§ C. Foudas,** B. J. King, W. C. Lefmann, W. C. Leung, S. R. Mishra,†† E. Oltman,† P. Z. Quintas, S. A. Rabinowitz, F. Sciulli, W. G. Seligman, and M. H. Shaevitz
Department of Physics, Columbia University, New York, New York 10027

R. H. Bernstein, F. O. Borcherding, H. E. Fisk, M. J. Lamm, W. Marsh, K. W. Merritt, P. A. Rapidis, and D. Yovanovitch
Fermi National Accelerator Laboratory, Batavia, Illinois 60510

P. H. Sandler and W. H. Smith
University of Wisconsin, Madison, Wisconsin 53706

(Received 2 August 1991)

We measure the energy loss of high-energy muons (up to 1 TeV) from cosmic-ray muons incident on the iron-scintillator calorimeter of the Chicago-Columbia-Fermilab-Rochester Collaboration (Lab E) neutrino detector at Fermilab. Measurements of the differential energy loss spectra in Fe and the average dE/dx energy loss in Fe are presented as functions of muon energy and are compared against calculations. There is reasonable agreement between the measurements and calculations except in the region of small energy losses (under a few GeV) for 1-TeV muons, where the measurement is about 30% lower than the calculation. This level of agreement with theory implies that reliable simulations of the performance of muon detectors for future TeV colliders can be done.

PACS number(s): 34.50.Bw, 25.30.Mr

I. INTRODUCTION

The processes by which a muon loses energy as it passes through matter are ionization, bremsstrahlung, direct e^+e^- pair production, and photonuclear interactions. The numerous ionization collisions with very small energy transfers produce a localized trail of ionization that is used by charged-particle detectors to obtain the muon's "track." In Landau's theory of energy loss by ionization [1], these numerous, small energy transfer collisions correspond to energy losses about the most probable value of the Landau distribution. The high-energy tail of the Landau distribution corresponds to stochastic collisions with large energy transfers (knock-on electrons). These higher-energy knock-on electrons produce electromagnetic shower cascades.

Cross sections for the production of knock-on electrons and for radiative and photonuclear interactions on atomic targets have been calculated for muons. They indicate that the amount of energy lost by a muon as it passes through matter increases as a function of the muon's energy, and that almost all of this increase is from radiative processes which are essentially stochastic. In this paper, we compare these predictions against our energy-loss measurements from a cosmic-ray exposure of the Chicago-Columbia-Fermilab-Rochester (CCFR) Collaboration neutrino detector at Fermilab [2].

The design of muon detectors for the Superconducting Super Collider (SSC) and of muon spectrometers for very-high-energy muon or neutrino scattering experiments requires a knowledge of these muon energy-loss mechanisms. Such detectors and spectrometers rely on active tracking elements to pick out the muon track. However, the muon track can be obscured by the presence of the cascade of secondary shower particles produced in muon interactions with sufficiently large energy losses. The frequency of such interactions is a key parameter in the design of these detectors and spectrometers. Detector design guidelines provided by computer simulations of the detector performance are only as reli-

*Present address: Northwestern University, Evanston, IL 60201.
†Present address: Lawrence Berkeley Laboratory, Berkeley, CA 94720.
‡Present address: National Center for Atmospheric Research, Boulder, CO 80307.
§Present address: Argonne National Laboratory, Argonne, IL 60439.
**Present address: University of Wisconsin, Madison, WI 53706.
††Present address: Harvard University, Cambridge, MA 02138.

able as the muon energy-loss cross sections used in the simulations. Thus it is important to test the reliability of these cross sections against measurements.

II. THE CCFR NEUTRINO DETECTOR

The CCFR neutrino detector (located in Lab E at Fermilab) is a 690-ton unmagnetized iron-scintillator target calorimeter followed by a 420-ton toroidal, magnetized steel, muon spectrometer. The target calorimeter is 17.7 m long and consists of 3 m×3 m steel plates interspersed with 2.54-cm-thick liquid scintillation counters and drift-chamber stations. The counters are placed every 10.3 cm of steel and the drift-chamber stations are placed every 20.6 cm of steel. The energy response and resolution of the calorimeter to hadrons and electrons have been measured using test beams. We have also measured the response of the calorimeter to low-energy (less than 9 GeV) minimum-ionizing muons using range-out muons from neutrino interactions. The calorimeter's response to hadronic showers (h), electromagnetic showers (e), and minimum-ionizing muons (μ) is different: the e/h and μ/h ratios are 1.11 and 1.34, respectively. The energy resolution for the minimum-ionizing, range-out muons is $\sigma_E/E \simeq 0.17$, where E is the muon's energy. The calorimeter's electromagnetic shower energy resolution is $\sigma_E/E \simeq 0.6/\sqrt{E}$, where E is the shower energy in GeV. For hadronic showers, the energy resolution is $\sigma_E/E \simeq 0.9/\sqrt{E}$.

The muon spectrometer consists of three, 1.75-m-radius, magnetized steel toriodal magnets with muon tracking drift-chamber stations. Its total length is 17.8 m. The total transverse momentum kick for a longitudinal track is 2.45 GeV / c and the angular resolution of the combined target calorimeter and toroid drift-chamber tracking system is about 0.3 mrad. The momentum resolution, which is limited by multiple Coulomb scattering in the steel, is $\delta(p)/p \simeq 11\%$. Additional details about the detector can be found in Ref. [2].

III. THE COSMIC-RAY MUON SAMPLE

The TeV muon energy-loss measurements are from cosmic-ray exposures of the CCFR neutrino detector taken during 1987 and 1988. The trigger selected muons that were nearly horizontal. Only muons that traverse the detector in the direction of the accelerator's neutrino beam and through the full length of the muon spectrometer are used. Events are required to be cleanly reconstructed in the muon spectrometer. The muon's momentum must be at least 9 GeV /c when it enters the muon spectrometer. For these events, the fractional momentum resolution is $\sigma_p/p \sim 0.11[1+(p/900)^2]^{1/2}$, where p is in GeV /c. Muon energy losses are measured in the calorimeter. To ensure proper energy-loss reconstruction with the scintillation counters, the muon track is required to be in a transverse fiducial region where the counter response is measured fairly well. As we are interested in energy losses of very-high-energy muons, muons that enter the calorimeter with energies less than 40 GeV are not used.

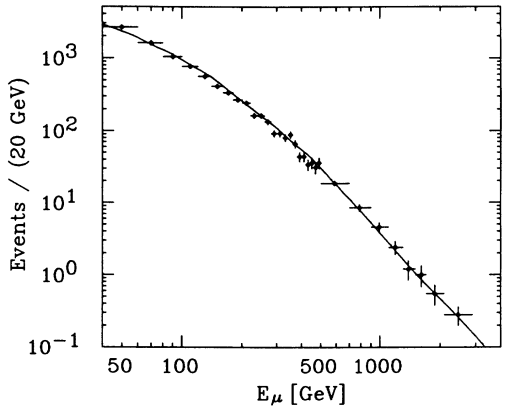

FIG. 1. The combined μ^+ and μ^- CCFR cosmic-ray muon spectrum. Between 500 and 800 GeV, 800 and 1200 GeV, 1200 and 2000 GeV, and 2000 and 3000 GeV, there are 236, 95, 43, and 13 events, respectively. Above 3000 GeV, there are six events. The solid curve is proportional to the differential muon flux measured by DEIS.

In the final event sample, there are 9411 events. The combined μ^+ and μ^- energy spectrum is shown in Fig. 1. For this event sample, the charge ratio of the number of μ^+ to μ^- events is 1.29±0.03. These measurements are consistent with previous cosmic-ray muon measurements from the DEIS [3] and MUTRON [4] spectrometers. MUTRON's charge ratio for muons arriving between 86° and 90° zenith angles is 1.251±0.005 for momenta less than 600 GeV /c and 1.30±0.02 for momenta above that. Our muon sample has an average zenith angle of 87°. The solid curve in Fig. 1 is proportional to the DEIS differential muon flux spectrum for zenith angles between 87 and 88°.

IV. ENERGY-LOSS CROSS SECTIONS

The cross sections which are used to predict the energy-loss spectra of muons incident on the CCFR target calorimeter are presented in this section. The radiative cross sections are analytic expressions based on detailed calculations that include atomic and nuclear form factors. Similarly, the photonuclear cross section is an analytic expression based on a calculation that includes nuclear shadowing. In this section, $c=1$: the units of mass, energy, and momentum are identical, e.g., GeV.

The collision, or ionization cross section, of a muon incident on an atom [5] is

$$\left[\frac{d\sigma}{dv}\right]_{\text{ion}} = Z\frac{2\pi r_e^2}{\beta^2 v^2}\frac{m_e}{E_\mu}\left[1-\beta^2\frac{v}{v_{\max}}+\frac{v^2}{2}\right]. \quad (1)$$

This is valid only for collisions where the momentum transfer to the atomic electron is large enough that it can be considered to be free of all bound-state and screening effects. In the equation, Z is the atomic number, m_e is the electron mass, E_μ is the incident muon energy, r_e is the classical electron radius, β is the incident muon's velocity relative to the speed of light, and v is the fraction

of the muon's energy transferred to the electron. The maximum fractional energy transfer is

$$v_{\max}=\frac{\beta^2}{1+(m_\mu^2+m_e^2)/2m_eE_\mu}\ , \tag{2}$$

where m_μ is the muon mass. The atomic electrons ejected in these collisions are called knock-on electrons.

The average ionization energy loss per unit length x (g / cm^2) is given by the Bethe-Bloch [5] formula

$$\left[\frac{dE}{dx}\right]_{\text{ion}}=2\pi r_e^2\frac{NZ}{A}\frac{m_e}{\beta^2}\left[\ln\frac{2m_eE_\mu\beta^2v_{\max}}{(1-\beta^2)I^2(Z)}-2\beta^2+\frac{1}{4}v_{\max}^2-\delta\right]. \tag{3}$$

In addition to the variables described previously, N is Avogadro's number, A is the atomic weight of the target, $I(Z)$ is the target's mean ionization potential [6,7], and δ is the density effect correction [6,7].

For muon bremsstrahlung on an atom, we use the Petrukhin-Shestakov cross-section formula [8]:

$$\left[\frac{d\sigma}{dv}\right]_{\text{brem}}=\alpha\left[2Zr_e\frac{m_e}{m_\mu}\right]^2\frac{1}{v}[1+(1-v)^2-\tfrac{2}{3}(1-v)]\phi(q_{\min})\ . \tag{4}$$

Here, $\alpha=1/137.036\ldots$, v is the fraction of the muon's energy transferred to the photon, and

$$\phi(q_{\min})=\ln\left[f_n\frac{m_\mu}{m_e}\frac{RZ^{-1/3}}{1+(q_{\min}/m_e)\sqrt{e}RZ^{-1/3}}\right], \tag{5}$$

where $f_n=\frac{2}{3}Z^{-1/3}$ is the nuclear form factor correction, $e=2.7182\ldots$, $R=189$, and $q_{\min}=m_\mu^2v/2E_\mu(1-v)$ is the minimum momentum transfer to the nucleus. The limits on the fractional energy transfer are taken to be

$$0<v\le 1-\frac{\sqrt{e}\,m_\mu}{2f_nE_\mu}\ . \tag{6}$$

Equation (4) is an analytic approximation to the Bethe-Heitler [9] bremsstrahlung cross section with arbitrary screening. To check this approximation, we have numerically evaluated the Bethe-Heitler cross section using a Thomas-Fermi atomic form factor in conjunction with a nuclear form factor from a two-parameter, Fermi nuclear charge density [10]. We find that the Petrukhin-Shestakov f_n underestimates by about 10% the numerical calculation and that nuclear size effects are better parameterized with $f_n=\exp(-0.128R_{0.5})$, where $R_{0.5}=1.18A^{1/3}-0.48$(fm) is the nuclear charge half radius. This latter correction is used in all calculations.

For the direct e^+e^- pair production by muons, we use the double differential expression derived by Kokoulin and Petrukhin [11]:

$$\left[\frac{d\sigma}{dv\,d\rho}\right]_{\text{pair}}=\frac{2}{3\pi}(Z\alpha r_e)^2\frac{1-v}{v}\times\left[\Phi_e(E_\mu,\rho,v)+\frac{m_e^2}{m_\mu^2}\Phi_\mu(E_\mu,\rho,v)\right], \tag{7}$$

where $\rho=(\varepsilon_+-\varepsilon_-)/(\varepsilon_++\varepsilon_-)$ is the e^+e^- energy asymmetry, $v=(\varepsilon_++\varepsilon_-)/E_\mu$, and $\varepsilon_+(\varepsilon_-)$ is the energy of the positron (electron). $\Phi_{e,\mu}(E_\mu,\rho,v)$ are given in the Appendix. The limits on the fractional energy transfer and the energy asymmetry are

$$0\le|\rho|\le\left[1-\frac{6m_\mu^2}{E_\mu^2(1-v)}\right]\left[1-\frac{4m_e}{vE_\mu}\right]^{1/2}, \tag{8}$$

$$\frac{4m_e}{E_\mu}\le v\le 1-\tfrac{3}{4}\sqrt{e}Z^{1/3}\frac{m_\mu}{E_\mu}\ . \tag{9}$$

Equation (7) is for an arbitrarily screened Thomas-Fermi atom with nuclear form-factor corrections (see the Appendix). In our calculations, the integration over ρ is done numerically. These formulas can also be used to estimate the rate of direct $\mu^+\mu^-$ pair production by muons [12]. While the resulting cross section is approximate because it does not include exchange effects, it indicates that $\mu^+\mu^-$ pair production can be neglected. At very small v where the differential cross section $(d\sigma/dv)$ for e^+e^- pair production is very large, the $\mu^+\mu^-$ cross section is highly suppressed due to mass-threshold effects The production of $\mu^+\mu^-$ pairs increases to about 10% of the e^+e^- level only when $v>0.5$. In this large v region, bremsstrahlung dominates all pair production.

The radiative cross sections, Eqs. (4) and (7), are for scattering in the field of a nucleus. This does not include incoherent scattering against individual nucleons within the nucleus or scattering against atomic electrons. In these processes, a virtual photon is exchanged with the target. Incoherent nucleon scattering can be neglected because the coherence length of the virtual photon, $\hbar c/q$, where q is the momentum transfer, is larger than the nuclear radius over most of the kinematic region. For example, the minimum momentum transfer ($q_{\min}$) of a 50-GeV muon is less than 2 MeV when $v<0.95$, and when $v>0.95$, it slowly increases from 2 to 106 MeV. Thus, incoherent scattering is not included in our calculations. To account approximately for bremsstrahlung and e^+e^- pair production on the atomic electrons, we replace the Z^2 in Eqs. (4) and (7) with $Z(Z+1)$.

For the photonuclear interactions of muons on nuclear targets, we use the results of calculations by Bezrukov and Bugaev [13]. They have calculated the effects of nucleon shadowing in the interactions of high-energy real and virtual photons using a generalized vector-dominance model. The expression they give is

$$\left[\frac{d\sigma}{dv}\right]_{\text{nucl}} = \frac{\alpha}{2\pi} A\sigma_{\gamma N}(vE_\mu)v\left\{0.75G(x)\left[\kappa\ln\left[1+\frac{m_1^2}{t}\right]-\frac{\kappa m_1^2}{m_1^2+t}-\frac{2m_\mu^2}{t}\right]+0.25\left[\kappa\ln\left[1+\frac{m_2^2}{t}\right]-\frac{2m_\mu^2}{t}\right]\right.$$
$$\left.+\frac{m_\mu^2}{2t}\left[0.75G(x)\frac{m_1^2}{m_1^2+t}+0.25\frac{m_2^2}{t}\ln\left[1+\frac{t}{m_2^2}\right]\right]\right\}, \quad (10)$$

where $\alpha=1/137.036\ldots$, A is the atomic weight, and v is the fraction of the muon's energy transferred to the nucleus in the interaction, $t=m_\mu^2 v^2/(1-v)$, $\kappa=1-2/v+2/v^2$, $m_1^2=0.54$ GeV^2, and $m_2^2=1.8$ GeV^2. The other functions are

$$\sigma_{\gamma N}(E)=114.3+1.647\ln^2(0.0213E)\ \mu b\ , \quad (11)$$

$$x=0.002\,82\,A^{1/3}\sigma_{\gamma N}(vE_\mu)\ ,$$

$$G(x)=\frac{3}{x^2}\left[\frac{x^2}{2}-1+e^{-x}(1+x)\right]\ . \quad (12)$$

Here, $\sigma_{\gamma N}(E)$ is the nucleon photonuclear cross section and E is in GeV. The limits on v are taken to be

$$\frac{m_\pi}{E_\mu}<v<1-\frac{m_\mu}{E_\mu}\ , \quad (13)$$

where m_π is the pion mass.

The ionization, bremsstrahlung, e^+e^- pair production, and photonuclear cross sections of 50- and 1000-GeV muons incident on an iron atom are shown in Figs. 2 and 3, respectively. The total pair production cross section per atom at those muon energies is 0.10 and 0.39 barn, respectively. The total ionization cross section per atom for energy losses larger than 1 MeV is practically independent of the muon energy and is equal to 6.6 barns. A visual scan of a sample of cosmic-ray event pictures confirm the general features of those figures. Events with higher muon energies contain more visible shower cascades. Very large energy showers and hadronic showers are observed, but they are relatively rare.

V. ENERGY-LOSS MEASUREMENTS

Muon energy losses are measured using the CCFR target calorimeter. A muon traversing the entire length of the calorimeter goes through 8.7 m of steel. The basic element in the calorimeter lattice is 10.3 cm of steel absorber followed by a scintillation counter and drift chambers with every other counter. In the energy-loss calculations and measurements, the scintillation counters and drift chambers are treated as an extra amount of steel absorber. There are three scaling lengths needed to convert the drift chamber and scintillator material to steel equivalents. For the ionization interaction, the scaling length is the distance of equivalent energy loss for minimum-ionizing particles. For the radiative interactions, the scaling length is the radiation length. For photonuclear interactions, the hadronic interaction length is taken as the scaling length. With the additional material, the basic element of the calorimeter lattice is on average

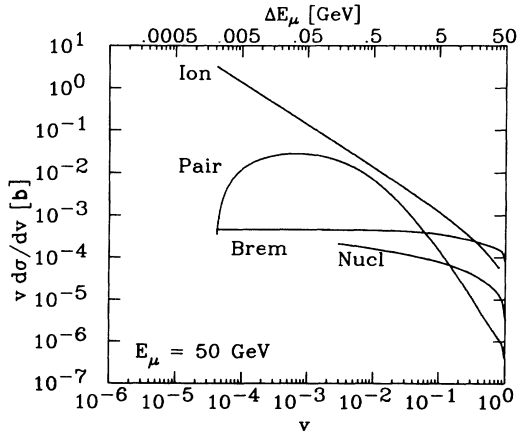

FIG. 2. The ionization, bremsstrahlung, pair production, and photonuclear cross sections of a 50-GeV muon incident on an iron atom. The top scale gives the muon energy loss ΔE_μ, which corresponds to the fractional muon energy loss v. Note that the ordinate is the logarithmic derivative $d\sigma/d(\ln v) = d\sigma/d(\ln \Delta E_\mu)$.

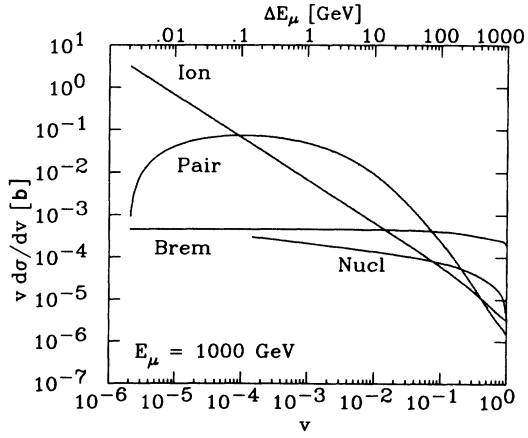

FIG. 3. The ionization, bremsstrahlung, pair production and photnuclear cross sections of a 1000-GeV muon incident on an iron atom. The top scale gives the muon energy loss ΔE_μ, which corresponds to the fractional muon energy loss v. Note that the ordinate is the logarithmic derivative $d\sigma/d(\ln v) = d\sigma/d(\ln \Delta E_\mu)$.

11.5, 10.6, and 11.7 cm of steel equivalent for ionization, radiative, and photonuclear interactions, respectively.

The 84 scintillation counters in the calorimeter are read out separately. This gives a longitudinal profile of a muon's energy loss as it passes through the calorimeter. Since the amount of material between counters corresponds to ~6 radiation lengths (~0.7 hadronic interaction lengths), energetic shower cascades can extend longitudinally more than one counter depth past the point of interaction. However, the probability of a muon producing two or more overlapping showers is not expected to be large. The calculated interaction lengths for producing showers larger than 0.25 GeV in iron for 10-, 100-, 1000-, and 5000-GeV muons are 510, 210, 65, and 34 cm, respectively.

The muon energy loss measured in a counter is the cumulative energy loss of many interactions, most of which are extremely small energy-loss ionizations. The occasional shower cascades from large energy-loss interactions are superimposed over this low-level ionization. These are from the knock-on electron, bremsstrahlung, direct e^+e^- pair production, and photonuclear interactions. We can measure the rate of these interactions by identifying and counting distinct showers in the calorimeter. The muon's average energy loss is extracted from the simple sum of scintillation counter energies.

The prediction for the average energy loss per unit length is obtained from the Bethe-Bloch formula [Eq. (3)] for ionization and from the integration of the other cross sections. The dE/dx for a process other than ionization is

$$\left[\frac{dE}{dx}\right]_p = E_\mu \frac{N}{A} \int_{v_{\min}}^{v_{\max}} v \left[\frac{d\sigma}{dv}\right]_p dv \ , \tag{14}$$

where N is Avogadro's number, A is the atomic weight, and p = brem, pair, or nucl. For elemental media, the total dE/dx is the simple sum of the dE/dx from ionization, bremsstrahlung, e^+e^- pair production, and photonuclear interactions. The dE/dx in iron of each process has been tabulated in Ref. [14] for muon energies between 1 and 10 000 GeV. In comparisons with our measurements, we have used the tabulations from this reference except for the bremsstrahlung process, which has been recalculated using a different nuclear form factor.

In the measurement of the dE/dx in steel, the cosmic-ray muons are sorted into momentum bins. A single muon track is split into an upstream and downstream section, which are assigned to different momentum bins if energy losses in the upstream region reduce the instantaneous momentum from one bin to another. The two measurements needed from each momentum bin are the cumulative path length of the muons and the corresponding total energy deposition ΔE. This energy is in units of "equivalent particles"[2] (EPs) (minimum-ionizing muons deposit about 1 EP per counter). Since the calorimeter's response is different for minimum-ionizing muons (low-energy-loss ionization), electromagnetic showers (radiative processes and ionization with energy loss larger than 0.25 GeV), and hadronic showers (photonuclear interactions), the total energy loss (ΔE) in a bin is separated into these components before being converted into an energy loss in GeV. To obtain the energy loss for the process p, we assume that the fraction of its energy loss relative to the total is equal to the theoretical value

$$f_p = \left[\frac{dE}{dx}\right]_p L_p C_p \Big/ \sum_i \left[\frac{dE}{dx}\right]_i L_i C_i \ , \tag{15}$$

where $(dE/dx)_p$ is the calculated dE/dx for process p, L_p is the corresponding total steel equivalent path length, C_p is the calibration constant from GeV to EP units of process p, and the sum over i runs over the two parts of the ionization, the radiation, and the photonuclear components. With this assumption the measured dE/dx for process p is $f_p \Delta E / L_p C_p$. The measurement along with the dE/dx prediction is shown in Fig. 4. The statistical errors on the dE/dx in Fig. 4 are the standard deviations from the expected total energy loss (ΔE) distributions. The theoretical formulas of the preceding section and the energy resolution functions of the CCFR target calorimeter are used to model the expected energy-loss distributions.

Shower cascades in the calorimeter are extracted from an event by examining the counter-by-counter longitudinal profile of a muon's energy loss as it traverses the calorimeter. In order to mask the fluctuating "background" of the low-level ionization energy loss prevalent in each counter, only structure above 0.5 GeV of minimum-ionizing equivalent energy loss per counter is retained for pattern recognition and the subsequent shower energy measurement. A contiguous cluster of counters each with energy above the threshold is treated as one shower cascade. Single, isolated counters with energies above the threshold are retained and also treated as a single shower. The stochastic energy loss $\Delta\varepsilon_s$, is defined to be the total energy deposited by the muon within the shower boundaries less the expected mean contribution from low-level ionization losses (~0.16 GeV of

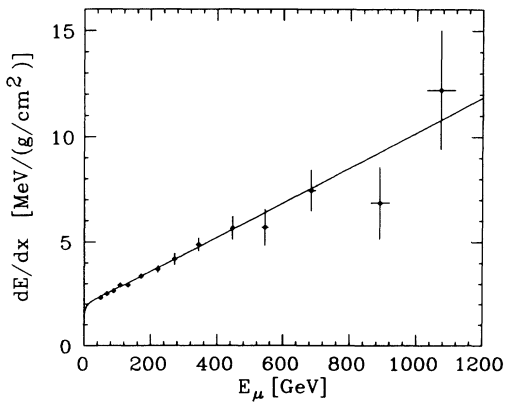

FIG. 4. dE/dx in steel for muons with energies between 40 and 1200 GeV. The solid curve is the theoretical prediction (fit χ^2 of 7 per 14 degrees of freedom). Systematic, shower energy calibration errors dominate the low E_μ points while the high-energy errors are statistical (see text). The 890-GeV and 1070-GeV points contain energy-loss samples from 5036 and 2853 counters, respectively.

minimum ionizing equivalent per counter).

Figures 5–9 show the stochastic energy loss for various ranges of the reconstructed muon energy. Also shown are the expected energy-loss distributions. The expected energy-loss spectra are calculated using the cross sections and the absolutely normalized muon flux of each energy range. The flux at energy E_μ is equal to the cosmic-ray flux (Fig. 1) at that energy times the fraction "smeared" by the finite resolution of the muon spectrometer into the energy range being considered. Because the total cross section without the minimum-ionizing part is still large, an apparent single shower observed in the calorimeter may be due to multiple interactions of the muon. This is taken into account with corrections to the single collision rates in the calculation. These corrections [15] are approximate and are significant for $\Delta\varepsilon_s$ of a GeV or less. The resulting expected energy-loss spectra are then convoluted with shower energy resolution functions, reconstruction efficiencies, and other reconstruction effects to give the predicted event distributions shown in Figs. 5 through 9.

The performance of the shower reconstruction is affected by the 0.5-GeV background suppression threshold that masks low-level ionization fluctuations. If the shower energy is very small, all of the shower cascade can be hidden under the threshold. Even if the central portion of a cascade is above threshold and is reconstructed, the peripheral regions at the longitudinal boundaries can dip beneath the threshold and not be reconstructed. Thus, the shower reconstruction is not fully efficient at low shower energies and there is some "missing energy" from portions of the shower under the threshold. For the dominant electromagnetic showers, we predict a reconstruction efficiency of 80% at 1 GeV and a missing energy of ~0.2 GeV with ~0.2 GeV rms fluctuations. In this 1-GeV or less region, the systematic errors on the predicted number of events are largest because of possible errors in modeling the threshold or uncertainties associated with the calorimeter's low-energy resolution. Of these, the largest contribution is from the missing-energy systematic error, which is taken to be 50 MeV. The corresponding error in the predicted number of events in Figs. 5 through 9 is given by the dotted curves in the low-energy-loss region.

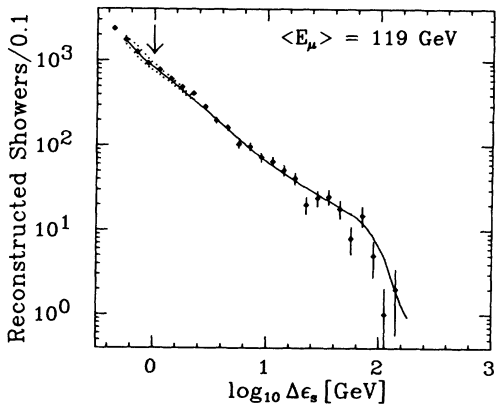

FIG. 6. Stochastic energy-loss distribution for muons between 80 and 180 GeV. The flux that produced these showers is equivalent to a muon penetrating through 223 200 counters (~11 cm Fe equivalent per counter). The smooth curve is the prediction described in the text. In the region to the right of the arrow, the fit χ^2 is 38 per 22 degrees of freedom.

Agreement between the measurements and predictions is reasonable for energy losses larger than 1 GeV, with the exception of the highest muon energy bin (Fig. 9) where the number of events is systematically lower than the predicted number of events for energy loss below 2 GeV. The kinematic region of low energy loss and high muon energy is interesting because it tests the e^+e^- pair production cross section (cf. Fig. 3). The dE/dx measurement, which has the virtue of being independent of the shower cascade analysis, is consistent with the

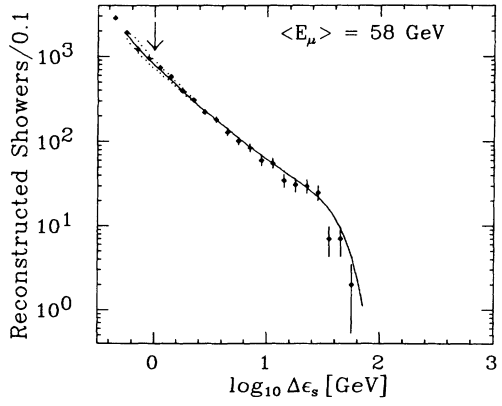

FIG. 5. Stochastic energy-loss distribution for muons between 40 and 80 GeV. The flux that produced these showers is equivalent to a muon penetrating through 299 400 counters (~11 cm Fe equivalent per counter). The smooth curve is the prediction described in the text. In the region to the right of the arrow, the fit χ^2 is 19 per 18 degrees of freedom.

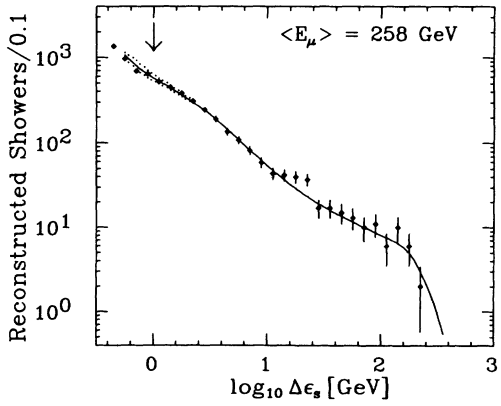

FIG. 7. Stochastic energy-loss distribution for muons between 180 and 400 GeV. The flux that produced these showers is equivalent to a muon penetrating through 106 700 counters (~11 cm Fe equivalent per counter). The smooth curve is the prediction described in the text. In the region to the right of the arrow, the fit χ^2 is 19 per 24 degrees of freedom.

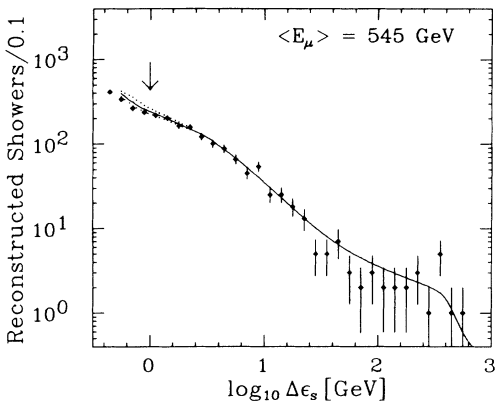

FIG. 8. Stochastic energy-loss distribution for muons between 400 and 800 GeV. The flux that produced these showers is equivalent to a muon penetrating through 32 150 counters (~11 cm Fe equivalent per counter). The smooth curve is the prediction described in the text. In the region to the right of the arrow, the fit χ^2 is 24 per 28 degrees of freedom.

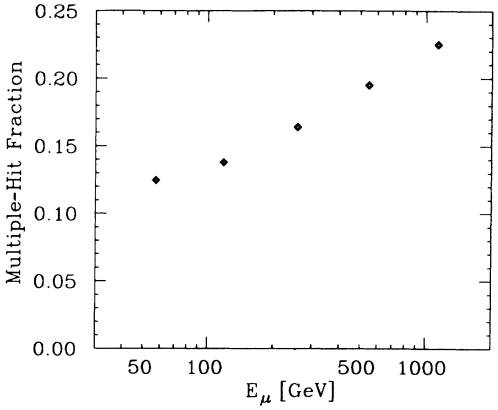

FIG. 10. The fraction of multiple flash ADC hits observed in the drift chambers for muon tracks as the function of muon energy. The hits are within 64 mm of the muon track. The muon energy is binned as in Figs. 5–9.

theoretical prediction. However, as the errors are large at high muon energies and since an excess such as the one in Fig. 9 produces an incremental dE/dx shift of ~5%, the dE/dx measurement cannot disprove this discrepancy either. Although this discrepancy is not understood, the implication is that detector design simulations which use the cross sections given in the previous section may somewhat overestimate the number of low-energy showers at the highest muon energies. At worst, the result is a more conservative detector design.

With increasing muon energies, the frequency of electromagnetic shower cascades increases. In steel, the central core of electromagnetic shower cascades is narrow and has a transverse size of ~1 cm. Such showers affect the identification and reconstruction of a muon's track because shower particles will obscure the muon whenever the particle tracking hardware cannot cope with the cascade particle density. The CCFR calorimeter has 42 drift chambers that are instrumented with multihit time-to-digital converters and flash analogue-to-digital converters (ADC's). Hit multiplicities in the 127-mm-wide drift-chamber cells are obtained using the flash ADC's, which can resolve particles separated by at least 2 mm. Figure 10 shows the fraction of multiple hits within 64 mm of a muon track as a function of the muon energy. The fraction of single hits in drift cells containing the muon track ranges from 90% for 40–80-GeV muons to 80% for 800–2000-GeV muons. Thus, even for 800–2000-GeV muons, the majority of drift cells on a muon's trajectory appear to have a single, minimum-ionization hits rather than multiple, shower cascade hits.

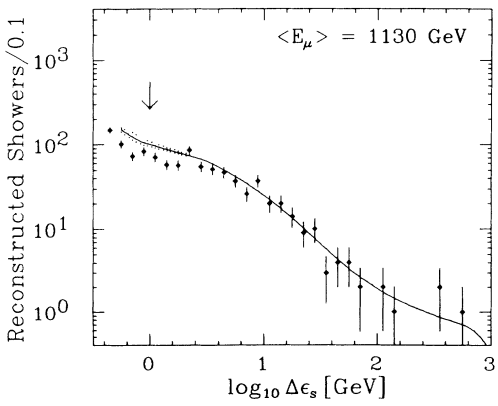

FIG. 9. Stochastic energy-loss distribution for muons between 800 and 2000 GeV. The flux that produced these showers is equivalent to a muon penetrating through 10 360 counters (~11 cm Fe equivalent per counter). The smooth curve is the prediction described in the text. In the region to the right of the arrow, the fit χ^2 is 40 per 23 degrees of freedom.

VI. SUMMARY

A muon loses energy as it passes through matter via ionization, bremsstrahlung, direct e^+e^- pair production, and photonuclear interactions. Through an exposure to cosmic-ray muons, the iron-scintillator target calorimeter of the CCFR neutrino detector was used to measure the energy losses in iron of muons whose energies ranged from 40 to 2000 GeV. The calculated average energy loss per unit length (dE/dx) agrees with the measurement. For energy losses larger than 1 GeV, there is fair agreement between the experimental energy-loss distributions and predictions based on the calculated cross sections. There is disagreement in the region of low energy loss and high muon energies. An earlier, high-statistics cosmic-ray experiment MUTRON [16] has also observed such a discrepancy for high-energy cosmic-ray muons, although at larger energy losses corresponding to $v \sim 0.01$. The interested reader is also directed to Ref. [16] for a

summary of results from other cosmic-ray experiments.

As the calculated cross sections are consistent with the measurements or are an upper bound to the measurements in regions of disagreement, they can be used in conjunction with electromagnetic and hadronic shower simulations to provide a realistic description for the transport of high-energy muons through matter. A Monte Carlo simulation that incorporates this muon transport would be a useful guide in the design of SSC detectors (e.g., see Ref. [17]). Tracking very-high-energy muons will become more and more difficult with increasing muon energies because of the increasing number of showers. The calculated interaction lengths for producing showers larger than 0.25 GeV in iron for 10-, 100-, 1000-, and 10000-GeV muons are 510, 210, 65, and 27 cm, respectively. The corresponding interaction lengths in uranium are 130, 28, 6, and 3 cm, respectively.

ACKNOWLEDGMENTS

We gratefully acknowledge the contributions of Jean Birkenmaier and Ken Gray for their invaluable technical assistance. We also thank the Fermilab staff, especially the Experimental Areas personnel, for their support. This work was supported in part by the U.S. National Science Foundation and Department of Energy. Rochester acknowledges support under DOE Contract No. DE-AC02-76-ER13065.

APPENDIX: e^+e^- PAIR PRODUCTION

The differential cross section for direct e^+e^- pair production is given in Eq. (7). The $\Phi_{e,\mu}$ functions in that equation are given below. The expression for L_e has been rearranged algebraically from that given in Ref. [11]:

$$\Phi_e=\left[[(2+\rho^2)(1+\beta)+\xi(3+\rho^2)]\ln\left[1+\frac{1}{\xi}\right]+\frac{1-\rho^2-\beta}{1+\xi}-(3+\rho^2)\right]L_e\ , \tag{A1}$$

$$\Phi_\mu=\left[\left[(1+\rho^2)(1+\frac{3}{2}\beta)-\frac{(1+2\beta)(1-\rho^2)}{\xi}\right]\ln(1+\xi)+\xi\frac{1-\rho^2-\beta}{1+\xi}+(1+2\beta)(1-\rho^2)\right]L_\mu\ , \tag{A2}$$

$$L_e=\ln\left[\frac{2}{3}\frac{m_\mu}{m_e}\frac{RZ^{-2/3}}{D_e}\right]-\frac{1}{2}\ln\left[1+\left[\frac{2}{3}\frac{m_\mu}{m_e}Z^{-1/3}\right]^2\frac{1}{(1+\xi)(1+Y_e)}\right]\ , \tag{A3}$$

$$L_\mu=\ln\left[\frac{2}{3}\frac{m_\mu}{m_e}\frac{RZ^{-2/3}}{D_\mu}\right]\ , \tag{A4}$$

$$D_{e,\mu}=1+\frac{q_{\min}}{m_e}\sqrt{e}RZ^{-1/3}(1+Y_{e,\mu})\ , \tag{A5}$$

$$Y_e=\frac{5-\rho^2+4\beta(1+\rho^2)}{2(1+3\beta)\ln(3+1/\xi)-\rho^2-2\beta(2-\rho^2)}\ , \tag{A6}$$

$$Y_\mu=\frac{4+\rho^2+3\beta(1+\rho^2)}{(1+\rho^2)(3/2+2\beta)\ln(3+\xi)+1-(3/2)\rho^2}\ . \tag{A7}$$

Here, $e=2.7182...$ and $R=189$. The parameters β, ξ, and $q_{\min}$ (minimum momentum transfer to the nucleus) are

$$\beta=\frac{v^2}{2(1-v)}\ ,\quad \xi=\left[\frac{m_\mu v}{2m_e}\right]^2\frac{1-\rho^2}{1-v}\ , \tag{A8}$$

and

$$q_{\min}=\frac{2m_e^2}{vE_\mu}\frac{1+\xi}{1-\rho^2}\ .$$

When $\rho=0$ and $v\simeq 0.01$, $q_{\min}$ is at its minimum and it is approximately equal to 110 keV (110 eV) for a 1-GeV (1-TeV) muon.

$\Phi_{e,\mu}$ are analytic approximations to pieces of the Kel'ner-Kotov [18] arbitrarily screened (Thomas-Fermi) Coulomb center cross section. Nuclear size effects are incorporated with corrections calculated using the two-parameter Fermi nuclear charge density form factor with negligible screening. We have done numerical calculations for an iron target using the more fundamental Kel'ner [19] cross section combined with a Thomas-Fermi atomic and a two-parameter Fermi [10] nuclear form factor to check the accuracy of Φ_e. These calculations and Φ_e agree to within 4%.

[1] L. Landau, J. Phys. U.S.S.R. **8**, 201 (1944).
[2] W. K. Sakumoto *et al.,* Nucl. Instrum. Methods **A294**, 179 (1990); B. J. King *et al., ibid.* **A302**, 254 (1991).
[3] O. C. Allkofer *et al.,* Nucl. Phys. **B259**, 1 (1985).
[4] S. Matsuno *et al.,* Phys. Rev. D **29**, 1 (1984).
[5] B. Rossi, *High-Energy Particles* (Prentice-Hall, Englewood Cliffs, NJ, 1952), p. 16.
[6] R. M. Sternheimer, S. M. Seltzer, and M. J. Berger, At. Data Nucl. Data Tables **30**, 261 (1984).
[7] R. M. Sternheimer, Phys. Rev. **103**, 511 (1956).
[8] A. A. Petrukhin and V. V. Shestakov, Can. J. Phys. **46**, S377 (1968).
[9] H. A. Bethe and W. Heitler, Proc. R. Soc. (London) **146A**, 83 (1934); H. A. Bethe, Proc. Cambridge Philos. Soc. **30**, 524 (1933). Also, see formula 3BS(b) (with the upper limits on the integrals extended from 1 to m_μ/m_e) in H. W. Koch and J. W. Motz, Rev. Mod. Phys. **31**, 920 (1959).
[10] H. R. Collard, L. R. B. Elton, and R. Hofstadter, in *Landolt-Börnstein, New Series, Group* I, *Vol. 2: Nuclear Radii,* edited by K.-H. Hellwege and H. Schopper (Springer-Verlag, Berlin, 1967).
[11] R. P. Kokoulin and A. A. Petrukhin, in *Proceedings of the 11th International Conference on Cosmic Rays,* Budapest, Hungary, 1969, edited by T. Gémsey *et al.* [Acta Phys. Acad. Sci. Hung. **29**, Suppl. 4, 277 (1970)]; in *Proceedings of the 12th International Conference on Cosmic Rays,* Hobart, Australia, 1971, edited by A. G. Fenton and K. B. Fenton (University of Tasmania, Hobart, 1972), Vol. 6, p. 2436.
[12] An estimate of $\mu^+\mu^-$ pair production by muons is obtained by replacing m_e with m_μ in all formulas, parameter definitions, and limits except in $L_{e,\mu}$ and $D_{e,\mu}$. The classical electron radius (r_e) is rescaled by m_e/m_μ. In L_e, R is replaced with Rm_μ/m_e.
[13] L. B. Bezrukov and E. V. Bugaev, Yad. Fiz. **33**, 1195 (1981) [Sov. J. Nucl. Phys. **33**, 635 (1981)].
[14] W. Lohmann, R. Kopp, and R. Voss, *Energy Loss of Muons in the Energy Range 1–10000 GeV* (CERN Yellow Report 85-03, European Organization for Nuclear Research, Geneva, Switzerland, 1985).
[15] Accounting for multiple interactions in the energy-loss distribution is complex. This has been done for the ionization process and it results in the Landau distribution. In calculating the expected energy-loss spectra, the ionization and e^+e^- pair production processes are corrected independently. The ionization correction is the difference between the knock-on electron rate and the Landau distribution normalized to the knock-on rate at $v_{\max}$; it is needed when $\Delta\varepsilon_s < 0.25$ GeV. The e^+e^- pair production correction is calculated via a Monte Carlo simulation. At an energy loss of a GeV, this correction is about 5% for 1-TeV muons and it decreases with decreasing muon energies.
[16] K. Mitsui *et al.,* Nuovo Cimento **A73**, 235 (1983).
[17] J. J. Eastman and S. C. Loken, in *Experiments, Detectors, and Experimental Areas for the Supercollider,* Proceedings of the Workshop, Berkeley, California 1987, edited by R. Donaldson and M. G. D. Gilchriese (World Scientific, Singapore, 1988), p. 542.
[18] S. R. Kel'ner and Yu. D. Kotov, Yad. Fiz. **7**, 360 (1968) [Sov. J. Nucl. Phys. **7**, 237 (1968)].
[19] S. R. Kel'ner, Yad. Fiz. **5**, 1092 (1966) [Sov. J. Nucl. Phys. **5**, 778 (1967)].